

# **A Toolbox for Unsupervised Change Detection Analysis**

Nicola Falco<sup>a</sup>, Prashanth Reddy Marpu<sup>b</sup> and Jon Atli Benediktsson<sup>c</sup>

<sup>a</sup> Faculty of Electrical and Computer Engineering, University of Iceland, Reykjavik, Iceland.

<sup>b</sup> Earth Observation and Hydro-Climatology Laboratory, Masdar Institute, Abu Dhabi, UAE.

## **Software description**

# Contents

<b>1</b>	<b>Introduction</b>	<b>2</b>
<b>2</b>	<b>ChangeDetection function (main function)</b>	<b>3</b>
<b>3</b>	<b>ITPCA / ITPCALine function</b>	<b>6</b>
<b>4</b>	<b>IRMAD / IRMADLine function</b>	<b>8</b>
<b>5</b>	<b>ICM / ICMLine function</b>	<b>10</b>
<b>6</b>	<b>WRM / WRMLine function</b>	<b>12</b>

# 1 Introduction

This tutorial describes the software which performs a change detection analysis on multispectral images. The function allows one to perform the cd analysis by choosing between two methods:

**ITPCA** is based on the application of the Iterated PCA (ITPCA) analysis.

By analyzing the 1st principal component, it is possible to find a linear relation between the two input images and perform a recalibration between them. A windows based misregistration recovery is apply to the re-calibrated images in order to correct small misregistration errors. The results of ITPCA could be improved by using a initial mask of the strong change, which pixel are excluded from analysis. On the re-calibrated and recovered images, the chi square analysis is applied by using EH algorithm, which performs a multidimensional gaussian mixture estimation of both changed and unchanged classes.

**IRMAD** method that performs a *Iteratively Reweighted Multivariate Alteration Detection*. The obtained canonical variates are filtered in order to correct the small misregistration errors. Then, the chi square analysis is applied in order to estimate the multidimensional gaussian mixture of both changed and unchanged class.

All the functions are described in the next sections.

## 2 ChangeDetection function (main function)

It is the main function. Here is possible to decide which method to use between ITPCA and IRMAD. For only the ITPCA method is possible to choose:

- type of processing: in case of a huge data set, is possible to apply a line by line processing, in order to save memory;
- initial change mask: in order to eliminate the strong change form the analysis, it is possible to create a initial change mask.

Syntax:

```
CD_IRMAD_ITPCA()  
CD_IRMAD_ITPCA(image_t1, image_t2, method)  
CD_IRMAD_ITPCA(image_t1, image_t2, method, opts, save_name, path_name)
```

opts for ITPCA:

$Tc$ ,  $flag\_plot$ ,  $size\_im$ ,  $flag\_mask$ ,  $low\_val$ ,  $dimWin$ ,  $flag\_save$

opts fro IRMAD:

$PCs$ ,  $epsln$ ,  $size\_im$ ,  $flag\_mask$ ,  $low\_val$ ,  $dimWin$ ,  $flag\_save$

Inputs:

- $image\_t1$ : string of the whole path of the ENVI bip format image at data t1;
- $image\_t2$ : string of the whole path of the ENVI bip format image at data t2;
- $method$ : string: choose between ITPCA and IRMAD;
- $save\_name$ : string of the name used as suffix when the files are saved;
- $path\_name$ : string of the path where to save the files;

opts for ITPCA (vector of integer)

- $Tc$ : convergence threshold for the ITPCA method (0.002 default value).

- *flag\_plot*: 0: no plot, 1: plot of the PCs.
  - *size\_im*: string: it permits to select a different processing in based on the dimension of the data set:
    - small images:  $\Rightarrow$  0: the whole data set is read.
    - big images:  $\Rightarrow$  1: the data set is read line by line (less memory used).
- 0: default value.
- *flag\_mask*: 1: to choose a strict mask thresholding based on EM algorithm, 2: to choose a relaxed mask thresholding based on EM algorithm, 3: to use the principal component instead of the original data set, 0: no mask. Default value = 0.
  - *low\_val*: value in to mask the low values of the histogram 0 no mask default value = 0.
  - *dimWin*: window dimension for the filter used in the WRMisreg function (e.g.: 3  $\Rightarrow$  for a 3x3 window, 5  $\Rightarrow$  for a 5x5 window, and so on (3 default value).
  - *flag\_save*: 0 to save the chi square files, 1 to save the chi square and the intermediary files.

#### **opts for IRMAD (vector of integer)**

- *PCs*: 0 to use the original dataset, 1 to use the principal components, default value = 0.
  - *epsIn*: epsilon for iterations. default value 0.05. Insert 100 to apply 0 iterations.
  - *size\_im*: string: it permits to select a different processing in based on the dimension of the data set:
    - small images:  $\Rightarrow$  0: the whole data set is read.
    - big images:  $\Rightarrow$  1: the data set is read line by line (less memory used).
- 0: default value.

- *flag\_mask*: 1: to choose a strict mask thresholding based on EM algorithm, 2: to choose a relaxed mask thresholding based on EM algorithm, 3: to use the principal component instead of the original data set, 0: no mask. Default value = 0.
- *low\_val*: value in to mask the low values of the histogram 0 no mask default value = 0.
- *dimWin*: window dimension for the filter used in the WRMisreg function (e.g.: 3 ⇒ for a 3x3 window, 5 ⇒ for a 5x5 window, and so on (3 default value)).
- *flag\_save*: 0 to save the chi square files, 1 to save the chi square and the intermediary files.

### Outputs:

- *ITPCA method (stored in ENVI bip format)*:
  - *ITPCA\_img1*: re-calibrated image t1.
  - *ITPCA\_img2*: re-calibrated image t2.
  - *PC1*: 1st principal component.
  - *PC2*: 2st principal component.
  - *rimg\_Diff*: difference between the re-calibrated images.
  - *wrm\_img*: misregistration recovery of the re-calibrated images.
  - *chi2\_itpca\_pc2*: 1st method: the Chi Square is obtained using the 2nd principal component.
  - *chi2\_itpca\_diff*: 2nd method: the Chi Square is obtained using the diff\_rim components.
  - *chi2\_itpca\_wrm*: 3rd method: the Chi Square is obtained using the wrm\_itp components.
  - *mask*: initial change mask.
- *IRMAD method (stored in ENVI bip format)*:
  - *cv1*: canonical variates1 unit variance.
  - *cv2*: canonical variates2 unit variance.
  - *mads*: the MAD variates.
  - *wrm\_img*: recovery misregistration of cvs.
  - *chi2\_irmad*: Chi Square obtained by using cvs.
  - *chi2\_irmad\_wrm*: Chi Square obtained by using the recovered cvs.

### 3 ITPCA / ITPCALine function

The Iterated PCA (ITPCA / ITPCALine) function performs a spectral re-calibration of the images based on the linear relation between them. The linear relation is related to the first principal component.

**Syntax:**

```
ITPCA()  
ITPCA(image_t1, image_t2)  
ITPCA(image_t1, image_t2, opts, save_name, path_name)  
opts for ITPCA:
```

*Tc, flag\_mask, low\_val, flag\_plot,*

**Inputs:**

- *image\_t1*: string of the whole path of the ENVI bip format image at data t1.
- *image\_t2*: string of the whole path of the ENVI bip format image at data t2.
- *save\_name*: string of the name used as suffix when the files are saved.
- *path\_name*: string of the path where to save the files.

**opts for ITPCA (vector of integer)**

- *Tc*: convergence threshold for the ITPCA method (0.002 default value).
- *flag\_mask*: 1: to choose a strict mask thresholding based on EM algorithm, 2: to choose a relaxed mask thresholding based on EM algorithm, 3: to use the principal component instead of the original data set, 0: no mask. Default value = 0.
- *low\_val*: value in to mask the low values of the histogram 0 no mask default value = 0.
- *flag\_plot*: 0: no plot, 1: plot of the PCs.

**Outputs:**

- *ITPCA\_img1*: re-calibrated image t1 / string of the whole path of the re-calibrated image t1 (line by line version).

- $ITPCA\_img2$ : re-calibrated image t2 / string of the whole path of the re-calibrated image t2 (line by line version).
- $PC1$ : 1st principal component / string of the whole path of 1st principal component.
- $PC2$ : 2st principal component / string of the whole path of 2nd principal component.
- (*stored in ENVI bip format*):
  - $ITPCA\_img1$ : re-calibrated image t1.
  - $ITPCA\_img2$ : re-calibrated image t2.
  - $PC1$ : 1st principal component.
  - $PC2$ : 2st principal component.
  - $mask$ : initial change mask.
- (*MATLAB structs*):
  - $ITPCA.mat$ : previous files in MATLAB format
  - $mask.mat$ :

## 4 IRMAD / IRMADLine function

Iteratively Reweighted Multivariate Alteration Detection.

**Syntax:**

```
IRMAD()  
IRMAD(image_t1, image_t2)  
IRMAD(image_t1, image_t2, opts, save_name, path_name)  
opts for IRMAD:
```

*PCs, epsln, flag\_mask, low\_val, w, flag\_save*

**Inputs:**

- *image\_t1*: string of the whole path of the ENVI bip format image at data t1;
- *image\_t2*: string of the whole path of the ENVI bip format image at data t2;
- *save\_name*: string of the name used as suffix when the files are saved;
- *path\_name*: string of the path where to save the files;

**opts for IRMAD (vector of integer)**

- *PCs*: 0 to use the original dataset, 1 to use the principal components, default value = 0.
- *epsln*: epsilon for iterations. default value 0.05. Insert 100 to apply 0 iterations.
- *flag\_mask*: 1: to choose a strict mask thresholding based on EM algorithm, 2: to choose a relaxed mask thresholding based on EM algorithm, 3: to use the principal component instead of the original data set, 0: no mask. Default value = 0.
- *low\_val*: value in to mask the low values of the histogram 0 no mask default value = 0.
- *w*: weights for stats calculation (available only for command line), 0 no weights. Default value = 0.

- *flag\_save*: 0 to save the chi square files, 1 to save the chi square and the intermediary files.

### Outputs:

- *cv1*: canonical variates1 unit variance. String of the whole path of the canonical variates cv1 (line by line version).
- *cv2*: canonical variates2 unit variance. String of the whole path of the canonical variates cv2 (line by line version).
- *mads*: the MAD variates. String of the whole path of the mads (line by line version).
- *chi2*: Chi Square. String of the whole path of the chi2 (line by line version).

## 5 ICM / ICMLine function

The Initial Change Mask (ICM / ICMLine) function identifies strong changes and creates a mask of them. The mask is produced by using the threshold estimated with EM algorithm.

**Syntax:**

```
ICM()  
ICM(image_t1, image_t2)  
ICM(image_t1, image_t2, flag_mask, low_val, save_name, path_name)
```

**Inputs:**

- *image\_t1*: string of the whole path of the ENVI bip format image at data t1.
- *image\_t2*: string of the whole path of the ENVI bip format image at data t2.
- *flag\_mask*: 1: to choose a strict mask thresholding based on EM algorithm, 2: to choose a relaxed mask thresholding based on EM algorithm, 3: to use the principal component instead of the original data set. Default value = 1.
- *low\_val*: value in to mask the low values of the histogram 0 no mask default value = 0.
- *save\_name*: string of the name used as suffix when the files are saved.
- *path\_name*: string of the path where to save the files.

**Outputs:**

- *mask*: initial change mask / string of the whole path of the initial change mask (line by line version).

### Example of results:

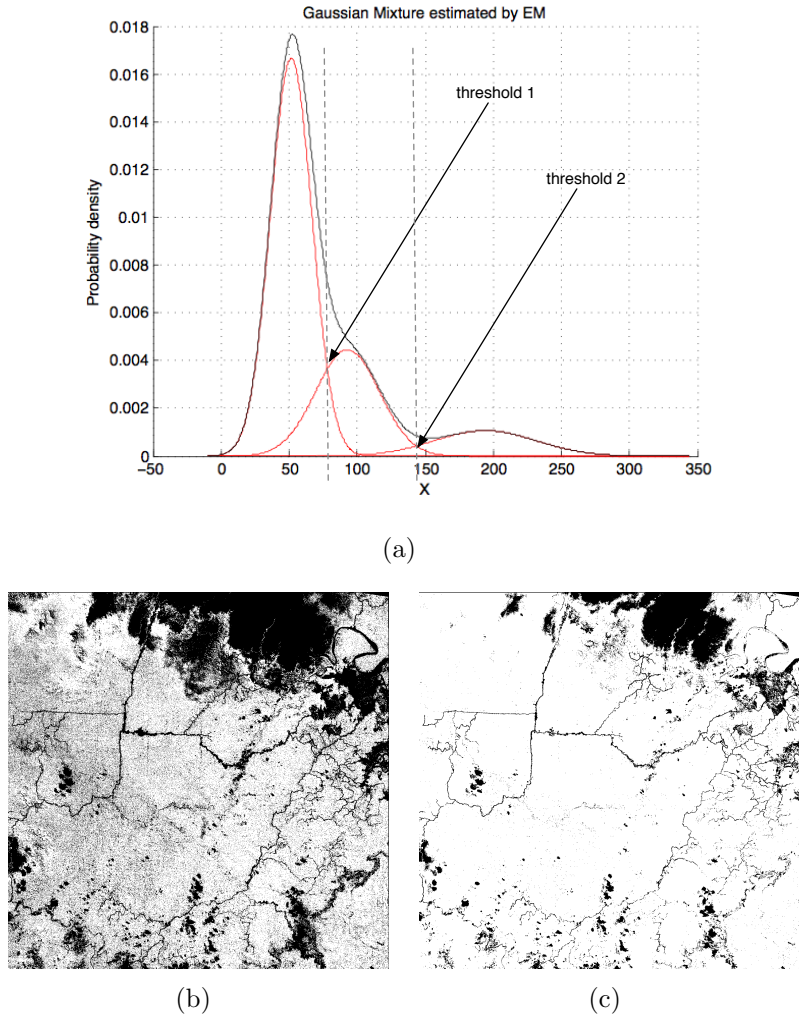


Figure 1: *Initial Change Masks obtained by using the 1st threshold(b), and the 2nd one(c). The pixels in black are excluded from further analysis as they represent strong changes.*

## 6 WRM / WRMLine function

The Window Recovery Misregistration (WRM / WRMLine) function performs a window-based correction for small misregistrations errors between two multitemporal and multispectral images.

**Syntax:**

```
WRM()  
WRM(image_t1, image_t2)  
WRM(image_t1, image_t2, dimWin, save_name, path_name)
```

**Inputs:**

- *image\_t1*: string of the whole path of the ENVI bip format image at data t1;
- *image\_t2*: string of the whole path of the ENVI bip format image at data t2;
- *dimWin*: window dimension for the filter used in the WRMisreg function (e.g.: 3 ⇒ for a 3x3 window, 5 ⇒ for a 5x5 window, and so on (3 default value);
- *save\_name*: string of the name used as suffix when the files are saved;
- *path\_name*: string of the path where to save the files.

**Outputs:**

- *wrm\_img*: recovered image / string of the whole path of the recovered image (line by line version);
- (*stored in ENVI bip format*):
  - *wrm\_img*: recovered image;
- (*MATLAB structs*):
  - *wrm\_img.mat*: recovered image

**Example of results:**

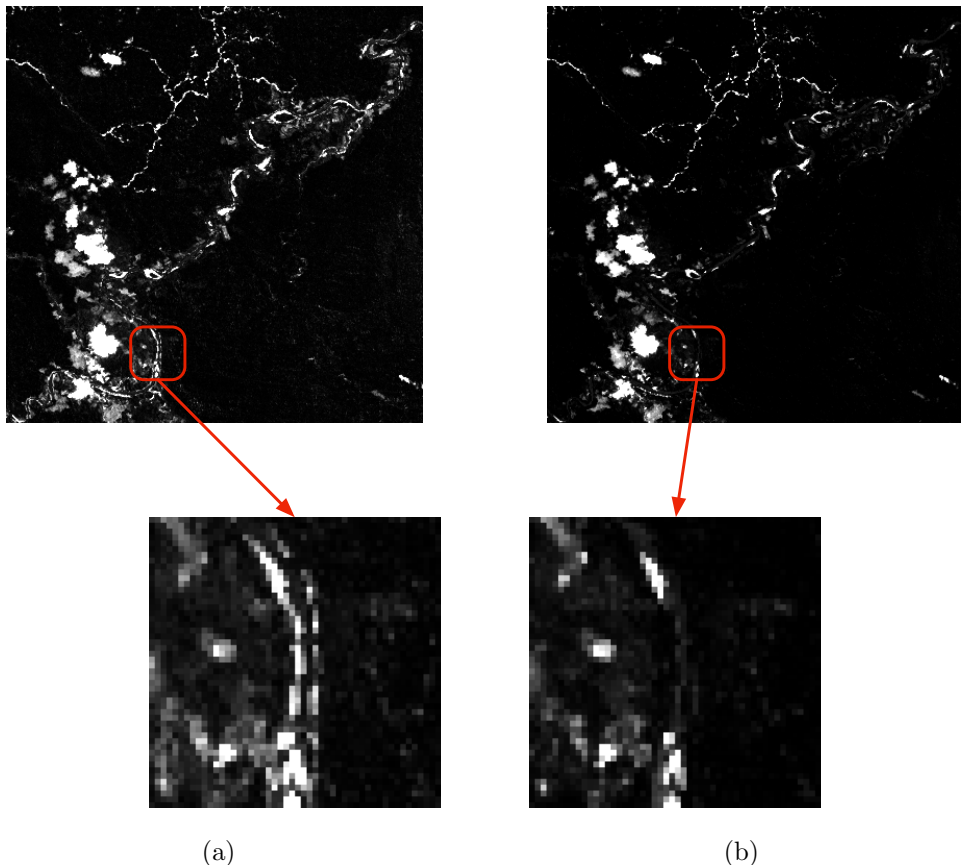
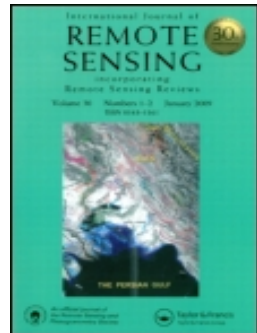


Figure 2: (a) (b) Without and with Window Recovery Misregistration.



## A toolbox for unsupervised change detection analysis

N. Falco, P. R. Marpu & J. A. Benediktsson

**To cite this article:** N. Falco, P. R. Marpu & J. A. Benediktsson (2016) A toolbox for unsupervised change detection analysis, International Journal of Remote Sensing, 37:7, 1505-1526, DOI: [10.1080/01431161.2016.1154226](https://doi.org/10.1080/01431161.2016.1154226)

**To link to this article:** <http://dx.doi.org/10.1080/01431161.2016.1154226>



Published online: 02 Mar 2016.



Submit your article to this journal 



View related articles 



View Crossmark data 

Full Terms & Conditions of access and use can be found at  
<http://www.tandfonline.com/action/journalInformation?journalCode=tres20>



## A toolbox for unsupervised change detection analysis

N. Falco <sup>a</sup>, P. R. Marpu<sup>b</sup> and J. A. Benediktsson<sup>a</sup>

<sup>a</sup>Faculty of Electrical and Computer Engineering, University of Iceland, Reykjavik, Iceland; <sup>b</sup>Institute Centre for Water and Environment, Masdar Institute of Science and Technology, Abu Dhabi, UAE

### ABSTRACT

The analysis of multi-temporal remote-sensing images is one of the main applications in Earth's observation and monitoring. In this paper, we present a Matlab toolbox for change detection analysis of optical multi-temporal remote-sensing data in which unsupervised approaches, iterative principal component analysis (ITPCA), and iteratively reweighted multivariate alteration detection (IR-MAD) are implemented and optimized. The optimization is represented by the implementation of novel pre- and post-processing strategies that aim to mitigate the side effects introduced by different acquisition conditions affecting change detection analysis. Special modules have been designed in order to decrease the required memory when large data sets are processed.

### ARTICLE HISTORY

Received 12 October 2015

Accepted 6 February 2016

## 1. Introduction

This work aims to present a toolbox, developed in Matlab<sup>®</sup> (© The MathWorks, Inc.) environment, where the unsupervised change detection methods of iterative principal component analysis (ITPCA) (Wiemker et al. 1997) and iteratively reweighted multivariate alteration detection (IR-MAD) (Canty and Nielsen 2006; Nielsen 2007; Canty 2014) are implemented, introducing a number of improvements aimed at assessing several issues in change detection analysis.

Unsupervised methodologies exploit image- and signal-processing techniques in order to characterize scenes without the use of additional information of the investigated areas, in contrast to supervised methodologies. The characterization is performed by extracting and identifying features and change measurements, which are able to highlight the differences between data. Several automatic pixel-based change detection techniques have been developed in the last decade based on different approaches (Bruzzone and Prieto 2000; Celik and Ma 2010; Chen et al. 2011). Change vector analysis (CVA) (Bovolo and Bruzzone 2007; Chen et al. 2011) identifies changes by computing the multi-spectral difference and uses the direction of the spectral change to perform change clustering. In Ghosh, Mishra, and Ghosh (2011) and Luo and Li (2011), fuzzy clustering and fuzzy-set theory are exploited to overcome the issue related to the overlap between change and no-change class.

Well-known methods employed in multi-spectral and hyperspectral anomalous change detection include chronochrome (Schaum and Stocker 1998), which is a linear prediction method that exploits the joint second-order statistics in order to find a linear transformation between two data sets, and covariance equalization (CE) (Schaum and Stocker 2004), which is an approximation of chronochrome where computation of the cross-covariance matrix is not involved. Methods based on linear transformations, such as maximum noise fraction (Celik 2009; Carty and Nielsen 2012) and independent component analysis (ICA), (Marchesi and Bruzzone 2009) have been also developed. A very good overview on change detection methods and approaches can be found in the recent work presented in Lu, Li, and Moran (2014).

The analysis becomes more complex due to the effects introduced by different acquisition conditions (Townshend et al. 1992; Chen 2007; Schowengerdt 2007), such as differences in illumination, acquisition angle, etc., which can affect the final result of the change detection analysis. In order to provide reasonable change detection maps and to mitigate these effects, methods based on a simple difference usually require pre-processing in which the multi-temporal data are calibrated and normalized.

In the literature, ITPCA and IR-MAD are well-known unsupervised change detection methods for multi-temporal multi-spectral images, being able to perform automatic radiometric normalization and mitigate side effects due to different acquisition conditions. In general, unchanged pixels are exploited for radiometric normalization between different acquisitions. However, if there is a large number of change pixels, the distribution of the unchanged pixels cannot be correctly estimated. In such cases, radiometric normalization is affected along with the discrimination between the change and no-change classes.

In this study, the problem is addressed by implementing a pre-processing phase, where the strongest changes are first identified (Marpu, Gamba, and Carty 2011) and subsequently ignored in the radiometric normalization stage. Another issue is misregistration error due to inaccurate co-registration between the considered multi-temporal data. Such error is usually identified as a change and propagated to the final result, increasing false alarms. In the toolbox described herein, this problem is tackled by implementing a novel strategy based on a local filtering analysis, which performs change detection considering the neighbourhood of each considered pixel.

In remote-sensing analysis, one of the main challenges is the analysis of large data sets which requires high computational resources. Moreover, the usual algorithms that are developed for Matlab® are designed in such way that images are loaded and saved in the workspace. This fact limits the use of such algorithms with large data sets due to the large amount of physical memory required. To overcome this problem, our toolbox implements line-by-line data processing where the workspace is used only for simple computations.

For demonstration, two real multi-temporal and multi-spectral remote-sensing images are considered for qualitative and quantitative analysis. The presented open-source toolbox is freely distributed under the GNU General Public Licence (<http://www.gnu.org/licenses/gpl.txt>).

## 2. Change detection analysis: background and improvements

This section provides the theoretical background of the ITPCA and IR-MAD methods for change detection, together with the recent developments and adaptations implemented in the toolbox.

### 2.1. ITPCA

The use of PCA for change detection analysis implies the assumption of a linear relation between no-change pixels belonging to the two acquisitions, where all the pixels can be separated into two main clusters along the principal axis. For simplicity, we report the formulation for the single-channel case and we extend it to the multi-spectral case.

Let us consider two single-band images,  $\mathbf{I}_1$  and  $\mathbf{I}_2$ , acquired over the same area at times  $t_1$  and  $t_2$ , respectively. By applying PCA, the information related to the unchanged regions is included in an elongated cluster along the first principal component,  $\text{pc}_1$ . Based on the initial assumption mentioned above, the line identified by the direction of  $\text{pc}_1$  can be considered as the correlation line between  $\mathbf{I}_1$  and  $\mathbf{I}_2$  and used for radiometric normalization between the two images. Here, the second principal component,  $\text{pc}_2$ , which is orthogonal to the first, can be used to quantify the change of a given pixel by computing the distance between that pixel and the correlation line.

An important issue that arises when PCA is used in this context is related to a non-correct estimation of the linear relation between the unchanged pixels ( $\text{pc}_1$ ). This is due to the incorrect computation of the covariance matrix, which is computed by considering all the unchanged and changed pixels, even though the assumption is valid only when unchanged pixels are considered or when the changed pixels are minimal.

In order to consider only unchanged pixels, an iterative scheme is used in which the distance between a given pixel and the correlation line computed at a given iteration is used to derive its weight. Such weight is exploited to compute the new correlation line in the next iteration (Wiemker et al. 1997). In more detail, the inverse of the magnitude of  $\text{pc}_2$ , which represents the distance from the correlation line, is used at each iteration as a weight,  $w_i$  for the computation of both the mean and covariance matrix. Thus, for each pixel  $p_i$  with  $i = 1, \dots, m$ , the weight  $w_i$  can be defined as follows:

$$w_i = \frac{1}{\sqrt{|p_{i,2}|}}, \quad (1)$$

where  $p_{i,2}$  is the value of the  $i$ -th pixel computed on the second principal component,  $\text{pc}_2$ . A pixel that is located far from the correlation line has a low probability of being unchanged, and has a low weight. In our formulation, the weights are first normalized, as follows:

$$w'_i = \frac{w_i}{\sum_{j=1}^m w_j}, \quad \text{such that } \sum_{i=1}^m w'_i = 1. \quad (2)$$

Considering the  $m \times 2$  data matrix  $\mathbf{X} = [\mathbf{X}_1, \mathbf{X}_2]$ , with  $\mathbf{X}_1$  and  $\mathbf{X}_2$  representing  $\mathbf{I}_1$  and  $\mathbf{I}_2$ , respectively, as column vectors of  $m$  elements, the unbiased weighted covariance matrix (Galassi et al. 2015) can be defined as:

$$\sum_{j,k} = \frac{\sum_{i=1}^m [w'_i (X_{i,j} - \bar{X}_k) (X_{i,k} - \bar{X}_k)]}{1 - \sum_{i=1}^m (w'_i)^2}, \quad (3)$$

where

$$\bar{X} = \sum_{i=1}^m w'_i X_i, \quad (4)$$

are the weighted means. PCA is then applied again by considering the computed covariance matrix, providing the new correlation line. In order to compensate for the contribution of the changed pixels, the process is repeated until convergence. Once the correlation line is found, its angular coefficient is used to perform calibration between the two images.

The analysis is extended to solve the change detection problem for multi-spectral data by applying the approach to all bands independently. The image difference,  $\mathbf{X}_{D,i}$ , between the calibrated data sets,  $\mathbf{X}_1^c$  and  $\mathbf{X}_2^c$ , is computed as:

$$\mathbf{X}_{D,i} = \mathbf{X}_{1,i}^c - \mathbf{X}_{2,i}^c, \quad (5)$$

with  $i = 1, \dots, N$  spectral bands. For each  $\mathbf{X}_{D,i}$ , based on the assumption of Gaussian mixture, three distributions (no-change, change, ambiguous) are estimated by exploiting the expectation maximization (EM) algorithm (Bazi, Bruzzone, and Melgani 2007), which provides the means and the variances. The Gaussian distribution of the no-change class is identified as that having the mean value closest to zero, and the variance of the no-change pixels is extracted from the relative covariance matrix. Let the random variable  $Z$  be the sum of the squares of calibrated image differences,  $\mathbf{X}_{D,i}$ :

$$Z = \sum_{i=1}^N \left( \frac{\mathbf{X}_{D,i}}{\sigma_{X_{D,i}}^{nc}} \right)^2, \quad (6)$$

where  $\sigma_{X_{D,i}}^{nc}$  is the variance of the no-change distribution used for normalization. The no-change observations are considered to be normally distributed and uncorrelated, making the realizations  $z$  of the random variable  $Z$  follow a  $\chi^2$  distribution with  $N$  degrees of freedom. The change probability can be defined as follows:

$$\Pr(\text{change}) = P_{\chi^2; N(z)}, \quad (7)$$

with  $P_{\chi^2; N(z)}$  representing the distribution function.

## 2.2. IR-MAD

Based on canonical correlation analysis (CCA) (Hotelling 1936; Lindquist and Picci 1996), the MAD (Nielsen, Conradsen, and Simpson 1998) method aims at identifying changes from the canonical difference of multivariate images. In MAD, the idea is to identify a linear transformation that minimizes the correlation between the canonical components of two acquisition times, thus aiming to maximize the change information.

Let us consider two  $N$ -band multi-spectral images acquired over the same region at different times,  $t_1$  and  $t_2$ , respectively. The two images can be represented by random vectors  $\mathbf{F} = [F_1, F_2, \dots, F_N]^T$ ,  $\mathbf{G} = [G_1, G_2, \dots, G_N]^T$ . The combined change information can be extracted by computing the difference  $\mathbf{D}$  as follows:

$$\begin{aligned} \mathbf{D} &= \mathbf{a}^T \mathbf{F} - \mathbf{b}^T \mathbf{G}, \\ \mathbf{a}^T \mathbf{F} &= a_1 F_1 + a_2 F_2, \dots, a_N F_N, \\ \mathbf{b}^T \mathbf{G} &= b_1 G_1 + b_2 G_2, \dots, b_N G_N. \end{aligned} \quad (8)$$

The change detection problem is formulated to identify the vectors  $\mathbf{a}$  and  $\mathbf{b}$  that maximize the variance  $V\{\mathbf{a}^T \mathbf{F} - \mathbf{b}^T \mathbf{G}\}$ , which in turn corresponds to determining linear combinations with minimum correlation. The estimation is computed by solving two generalized eigenvalue problems for the CCA coupled via the parameter  $p$  as follows:

$$\begin{aligned} \sum_{FG} \sum_{GG}^{-1} \sum_{FG}^T \mathbf{a} &= \rho^2 \sum_{FF} \mathbf{a}, \\ \sum_{FG}^T \sum_{FF}^{-1} \sum_{FG} \mathbf{b} &= \rho^2 \sum_{GG} \mathbf{b}, \end{aligned} \quad (9)$$

where  $\Sigma_{FF}$  and  $\Sigma_{GG}$  are the covariance matrices of  $\mathbf{F}$  and  $\mathbf{G}$ , respectively, and  $\Sigma_{FG}$  is the cross-covariance matrix between  $\mathbf{F}$  and  $\mathbf{G}$ . The MAD transformation is defined as follows:

$$\mathbf{M}_i = \mathbf{a}_i^T \mathbf{F} - \mathbf{b}_i^T \mathbf{G}, \quad (10)$$

where the quantities  $a_i^T F, b_i^T G$  are denoted as canonical variates (CVs), and  $\mathbf{M}_i$  identifies the  $i$ -th MAD variate. The canonical and the MAD variates are mutually uncorrelated.

Let the random variable  $Z$  be the sum of the squares of standardized MAD variates:

$$Z = \sum_{i=1}^N \left( \frac{\mathbf{M}_i}{\sigma_{M_i}^{nc}} \right)^2, \quad (11)$$

where  $\sigma_{M_i}^{nc}$  is the variance of the no-change distribution used for normalization. The change probability can be defined as follows:

$$\Pr(\text{change}) = P_{\chi^2; N(z)}, \quad (12)$$

where  $\chi^2$  represents the chi-square distribution with  $N$  degrees of freedom.

An improvement on the MAD approach is iteratively reweighted (IR)-MAD (Nielsen 2007). In order to increase the detection of observations whose status over time is uncertain, high weights are put on observations that exhibit little change. This is done by using the probabilities of no-change as weights, which are then used to compute the covariance matrix using Equation (3) in the next iteration. Thus, at each iteration a better no-change background is identified, achieving a better separability between the change and no-change classes.

### 2.3. Pre-processing: strongest changes and dark region detection

The two aforementioned techniques address the change detection problem by identifying the unchanged pixels which are used for radiometric normalization. As shown by Marpu, Gamba, and Cantz (2011), IR-MAD fails when the unchanged pixels are few in number compared to the changed pixels, making it difficult to achieve accurate radiometric normalization.

Let us consider three different classes, namely unchanged, soft change, and strong change pixels. The improvement proposed by Marpu, Gamba, and Carty (2011) is to first identify the strongest changes and eliminate these from further analysis, providing the so-called initial change mask (ICM). In this way, when IR-MAD and ITPCA are applied, only the pixels related to the no-change class and soft change classes are considered, making radiometric normalization easier to achieve (Falco, Marpu, and Benediktsson 2012).

The identification of strong change is here implemented considering two different strategies, described in Sections 2.3.1 and 2.3.2. The first strategy is based on the analysis of the histogram of the data set (Marpu, Gamba, and Carty 2011), whereas the second considers the information extracted by performing a principal component analysis (Marpu, Gamba, and Benediktsson 2011).

Another issue arises when a large number of dark pixels, which are usually related to regions of water and shadows, is present in the scene. The computation of the covariance matrix is affected, resulting in a non-correct estimation of the distribution of the change and no-change classes. Therefore, this method aims to identify and eventually exclude dark regions from the change detection analysis. The selection of dark regions is based on the analysis of the histograms computed on each band that composes the data set. Such regions are located in the first low values in the histogram, and are data-variant. The process requires the user to enter the percentage of low values that has to be excluded from the change detection analysis.

### **2.3.1. ICM based on the threshold of bin differences**

This approach is based on the analysis of the image histogram with the assumption that unchanged pixels preserve their position in the histogram, and the changes are detected by histogram difference Marpu, Gamba, and Carty (2011). According to this, let  $X_1$  and  $X_2$  be two multi-spectral multi-temporal images. The images are first linearly stretched over the range of values between 0 and 255 and the difference is computed between the two acquisitions, band by band. In order to find the strongest changes, meaning those pixels with high probability are changed, the maximum difference in absolute value for each pixel calculated over all bands is found.

To minimize the effect of overlapping between the change and no-change classes (Ghosh, Mishra, and Ghosh 2011), the resulting difference image,  $X_D$ , is modelled as a mixture of three Gaussian distributions by using the EM algorithm. These distributions are related to the purely no-change, ambiguous, and pure change classes, where the Gaussian of the no-change is that closest to zero. The threshold, which discriminates the component of strong change, corresponds to the boundary between the first and second distributions, as shown in Figure 1(a), and it is used to build the ICM.

### **2.3.2. ICM based on the first PC**

The ICM approach is based on PCA linear transformation. The analysis is applied to the difference between two multi-spectral images,  $X_1$  and  $X_2$ , resulting in a difference image,  $X_D$ , with the same spectral dimension. For the estimation of the Gaussian distribution, the EM algorithm is applied to the first PC, which is the component with the highest variance. As in the previous case, we need to identify the thresholds between the class distributions. In this case, the class of unchanged pixels is associated with the

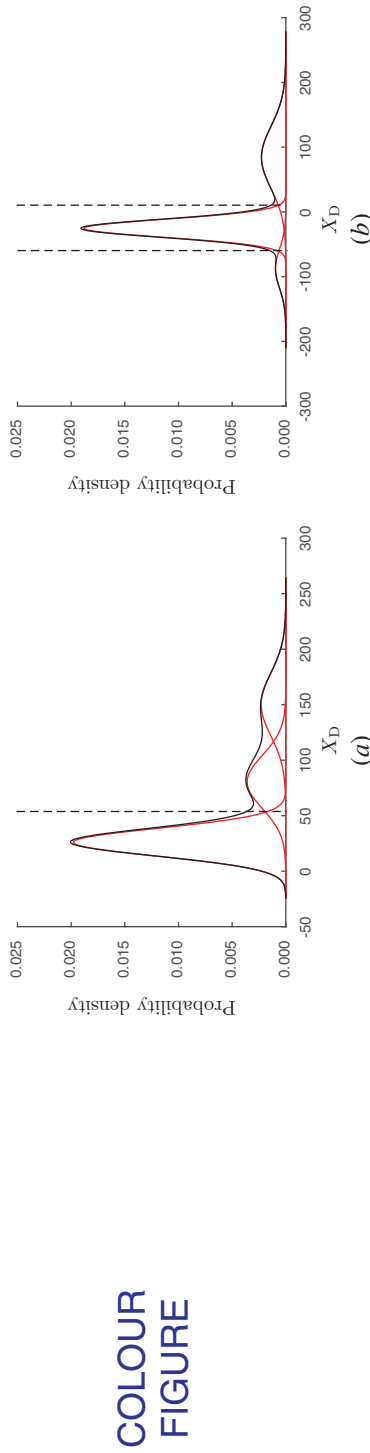


**Figure 1.** Estimation of the distribution of change and no-change classes for the difference image obtained by the two algorithms of ICM. The no-change class is represented by Gaussian distribution with the mean value closest to zero. (a) Approach based on the threshold of bin differences; (b) approach based on the first principal component.

distribution with mean value closest to zero, positioned in the middle. Thus, to build the ICM, we need to identify the left and right boundaries of the distribution, as shown in Figure 1(b).

#### 2.4. Post-processing: minimization of misregistration error

A very common problem in change detection analysis is misregistration error. Change detection analysis is usually based on the assumption that pixels that belong to the image at time  $t_1$  correspond to the pixels in the image at time  $t_2$  with the same spatial ordering. In order to achieve optimal alignment of two or more remote-sensing images acquired over the same area, a co-registration process is usually performed. However, minor displacements could still remain after such analysis, which appear as changes in the final map.

In the proposed toolbox, a floating window search approach called the window recovery method (WRM) is developed in order to reduce minor misregistration errors. The method implemented here is similar to that presented by Theiler and Wohlberg (2012), where symmetric local co-registration adjustment (SLCRA) is used for anomalous target detection and the operator ‘min’ is used to compare a single pixel of  $X_1$  to a pixel in the same position in  $X_2$  and its neighbourhood pixels, and to detect anomalous changes after the co-registration phase. The method proposed here (shown in Figure 2), performs comparison in a similar way but on statistically similar entities, such as CVs in the case of IR-MAD and radiometric calibrated images in the case of ITPCA. WRM compares the value of a given pixel  $p_j^{t_1}$  belonging to the image  $t_1$  to the same pixel in the image  $t_2$  by also considering the neighbourhood pixels, which are defined by the floating window,  $\mathbf{W}^{t_2}$ , as it follows:

$$D_j^{t_1} = \min \left\{ \left| p_j^{t_1} - \mathbf{W}^{t_2} \right| \right\}. \quad (13)$$

The process is repeated in the opposite direction, between  $p_j^{t_2}$  belonging to image  $t_2$  to the same pixel in the image  $t_1$  considering the neighbourhood pixels, which are defined by  $\mathbf{W}^{t_1}$  as follows:

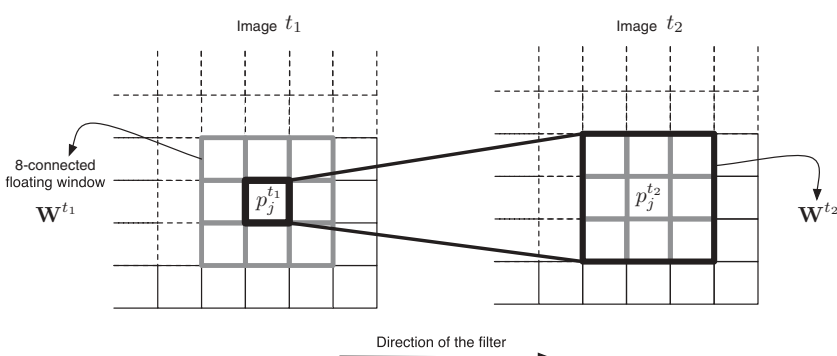


**Figure 2.** WRM: computation of  $D_j^{t_1}$ , which is obtained by comparing pixel  $p_j^{t_1}$  in image  $t_1$  and  $\mathbf{W}^{t_2}$  defined for the image  $t_1$ . The process is then repeated in the opposite direction, obtaining  $D_j^{t_2}$ . The final value of  $p_j$  corresponds to the maximum between the two subtractions,  $D_j^{t_1}$  and  $D_j^{t_2}$ .

$$D_j^{t_2} = \min \left\{ \left| p_j^{t_2} - \mathbf{w}^{t_1} \right| \right\}. \quad (14)$$

The final value of  $p_j$  corresponds to the maximum between the two subtractions:

$$p_j = \max \left\{ D_j^{t_1}, D_j^{t_2} \right\}. \quad (15)$$

In this formulation, the idea is to perform image differentiation promoting the analysis between pixels of similar value. The differentiation between pixels affected by displacement would be minimized, depending on the size of the window.

The size of the floating window is a parameter that has to be estimated by the user and should be large enough to cover the expected misregistration error. It is worth noting that this post-processing phase is optional and it is meant to minimize minor misregistration errors, with the assumption that the area of change region is greater than that affected by misregistration. Moreover, the increase in window size means an increase in the computational cost of such analysis, and can also lead to errors, with the risk of missing changes that are smaller than the window size. The effect obtained by performing the WRM algorithm is shown in [Section 4.4](#).

### 3. Description of the software

The software was developed in the Matlab® environment. In [Figure 3](#), the general scheme of the change detection process is depicted.

#### 3.1. Description of the inputs

The software is provided with an interactive input selection. The interactive menu queries the user to choose the multi-temporal data sets, the change detection technique to use, the different parameters needed in the pre-processing, the processing modality, and the location for saving the files created during the process. The software reads ENVI format input images, which consist of binary files coupled with a header file that contains all the metadata related to the data set.

In pre-processing, the software requests the user to indicate whether ICM is required and, if so, which approach (see [Section 2.3](#)) to use for the computation of the mask. The ICM has two important roles, one related to the detection of strong changes to improve radiometric normalization, and the selection of dark regions to avoid bias. In this case, the user has to indicate the percentage of the cumulative histogram that has to be filtered out.

In post-processing, it is possible to minimize the misregistration error via the WRM function. In this case, the software asks the user to indicate the dimension of the floating window used as filter.

#### 3.2. Analysis of large data sets

Due to the limited physical memory, many algorithms for change detection are designed and tested on small data sets, which are usually stored in the workspace. In order to analyse large data sets we need to identify an efficient strategy (in-line strategy)

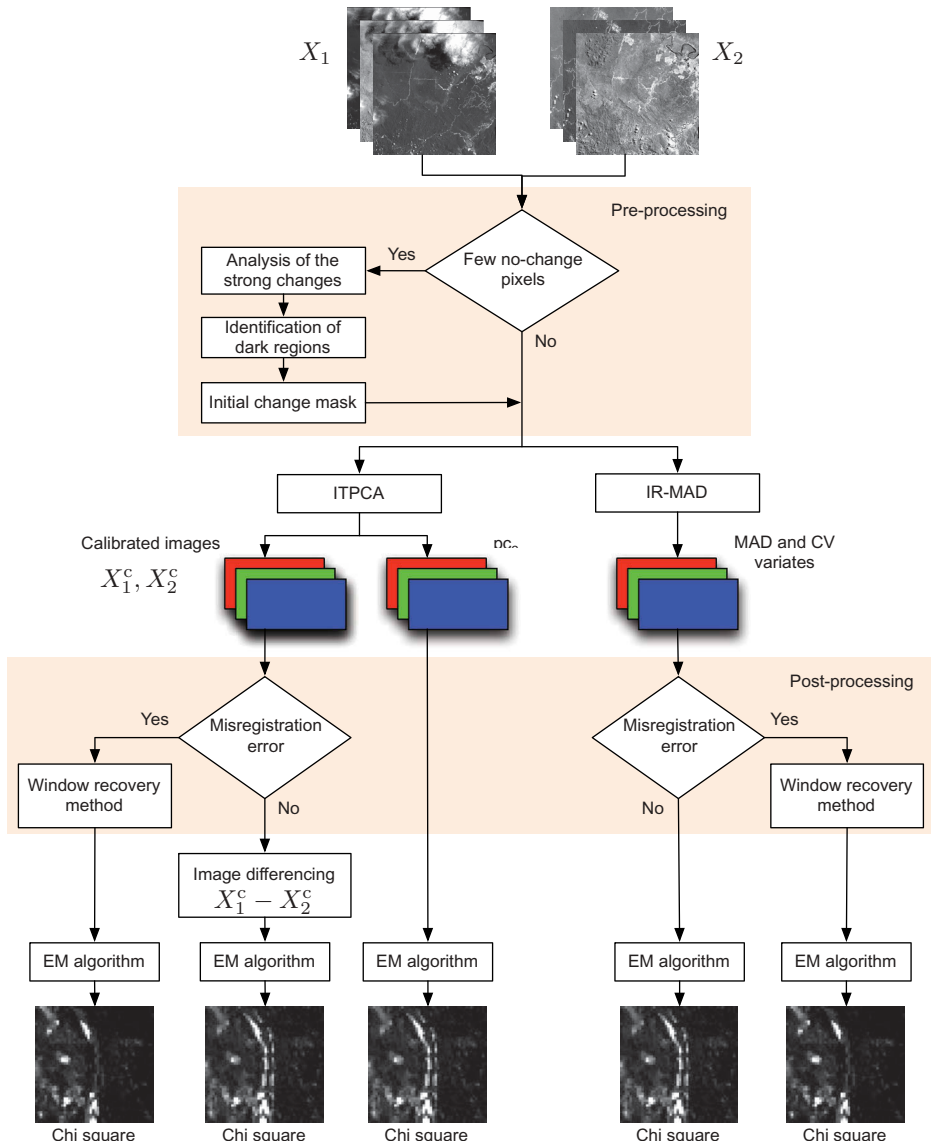


**Figure 3.** General scheme of the toolbox.

that avoids the use of the workspace, which has limitations in terms of available memory.

For this purpose, the input images are converted to a band-interleaved-by-pixel (BIP) format, which allows this strategy to be easily implemented, and all the bands to be processed at the same time. This strategy is reasonable for every simple algebraic computation but becomes complicated when we need to compute statistics, which needs the information of the entire data set, such as the computation of means and covariance matrices.

In order to compute statistics by reading and processing the images line by line, the method of provisional means (Dixon 1981; Carty 2006; Vokey and Allen 2011) was used. This refers to a recursive method for computing a mean. This method has been implemented and extended for the computation of the means, covariance matrices, and weighted covariance matrices. A comparison of the computational time between the strategy normally used for small data sets and the in-line strategy is provided in Section 4.4.

## 4. Demonstration and discussion

In this section, the data sets used in the experiments are described and the experimental results are discussed. For demonstration purposes, the analysis is performed on multi-spectral data sets. However, the software provides the potential also to process hyperspectral images. As the IR-MAD method is affine to linear transformation, this provides a direct way to provide an extension to hyperspectral images through linear transformations like PCA (Marpu, Gamba, and Benediktsson 2011), which is employed for feature reduction.

### 4.1. Data set description

To explore the utility of the proposed toolbox, two different real data sets, both acquired by the Landsat Enhanced Thematic Mapper Plus (ETM+) sensor, are considered for the analysis.

#### 4.1.1. Germany

The multi-temporal data set is composed of two multi-spectral images acquired over the city of Jülich, Germany, on 25 May and 26 June, respectively, in the year 2001. The images have a size of  $1000 \times 1000$  pixels, with a spatial resolution of 28.5 m. The data set originally included seven spectral bands but band 6, which represents the thermal infra-red channel, is excluded. The final data set consists of six spectral bands [1–5 and 7]. The scene shows a vast agriculture area, including several urban areas, such as the cities of Jülich (in the centre), Düren (southeast), and Eschweiler (south-west), and two opencast mining areas (in white–grey). Here, the main change is due to agriculture activity. Figure 4 shows a RGB composite of the multi-temporal data set. For testing purposes, reference data manually defined by Marpu, Gamba, and Carty (2011), which consists of 9521 changed pixels and 13,911 unchanged pixels, are used as shown in Figure 4(c).

#### 4.1.2. Indonesia

The multi-temporal data set was acquired over the Labanan concession forest in Berau municipality, East Kalimantan Province, Indonesia. The two ETM data sets were acquired on 26 August 2000 and 31 May 2003, respectively. The scene has a size of  $400 \times 400$  pixels with spatial resolution of 30 m. Figure 5 shows a false-colour composite of the multi-temporal data set. As in the German data set, band 6 is also excluded for further analysis. The data set is here used as a showcase for evaluation of the WRM algorithm.

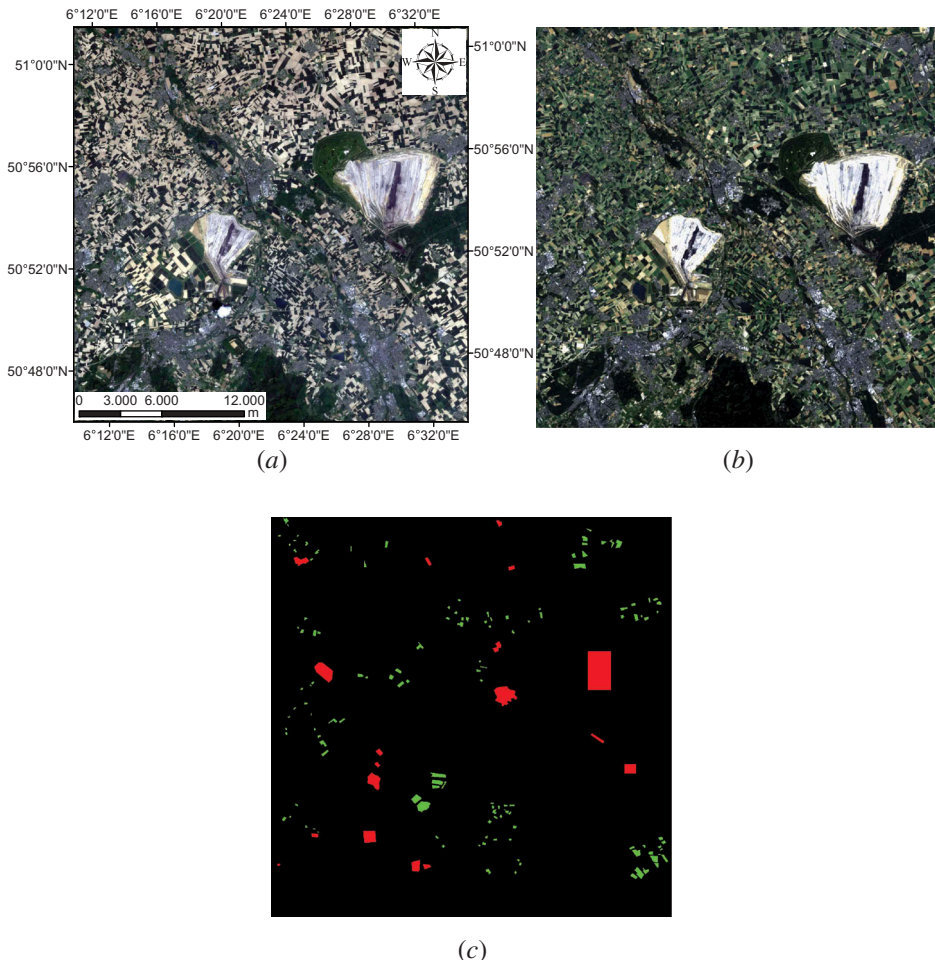


**Figure 4.** RGB composite (bands 3, 2, 1) of the image acquired over the city of Jülich, Germany: (a) 25 May 2001; (b) 26 June 2001. (c) Reference map: no-change class is in red and the change class in green.

#### 4.2. Pre-processing analysis

Considering the scheme in Figure 3, the first (optional) step is to perform pre-processing in which the strongest changes and the darkest regions are identified and masked by creating an ICM. Figure 6 shows the ICMs obtained by applying both strategies to the German data set, where the pixels in black represent strong changes and are excluded from further analysis.

As can be seen, the two approaches provide different initial masks. This is due to the fact that the histogram analysis-based strategy takes into account the information of the whole data set, while the second strategy only considers the information extracted from the first PC. For both approaches the thresholds that provide the change detection mask are identified by using the EM algorithm, which estimates the class distribution by considering 50,000 pixels randomly selected over the whole image.

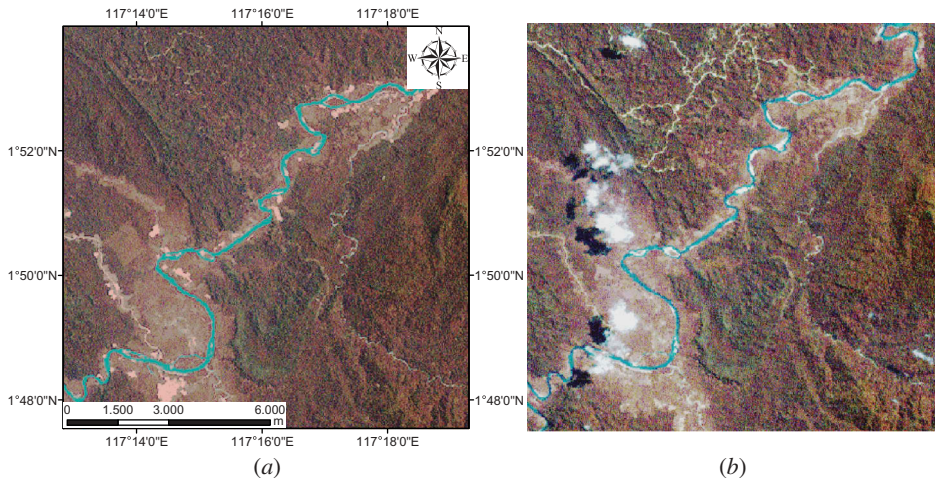


**Figure 5.** False-colour composite (bands 4, 2, 1) of the image acquired over Berau municipality, Indonesia. (a) 26 August 2001; (b) 31 May 2003.

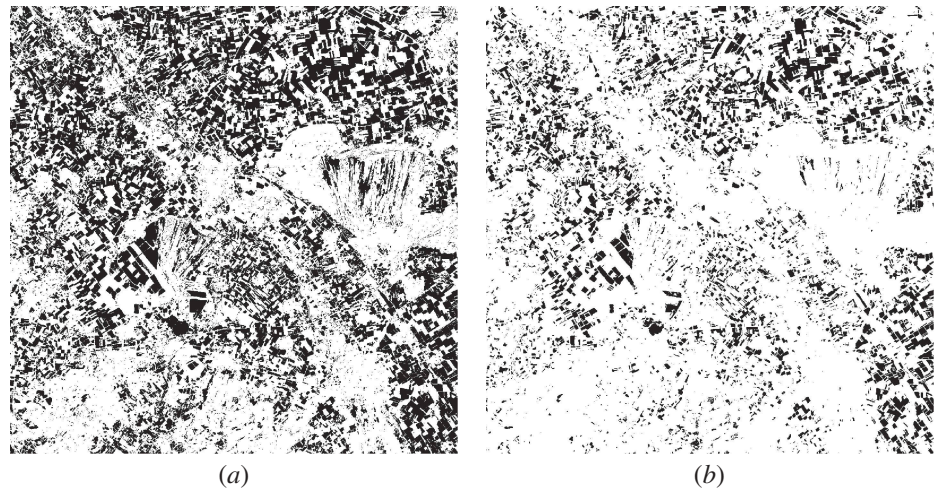


**Figure 6.** Example of ICMs computed for the German data set. (a) ICM based on the threshold of bin differences; (b) ICM based on the first principal component. The pixels in black represent strong changes and are excluded from further analysis.

#### 4.3. Change detection analysis

Change detection analysis is performed by one of the two methods, IR-MAD or ITPCA. Figure 7 shows the results obtained by the two techniques. In the case where ICM is not employed for masking the strongest changes, both approaches provide chi-square images where unchanged regions (e.g. parts of the opencast mining areas) are wrongly selected as changes.

The chi-square images obtained by using the two ICM approaches are quite similar (Figures 7(b) and 7(e)) show the case where ICM based on the threshold of bin differences is used; Figures 7(c) and 7(f) show the case where ICM based on the first principal component is used), where the distribution of both the change and no-change classes is

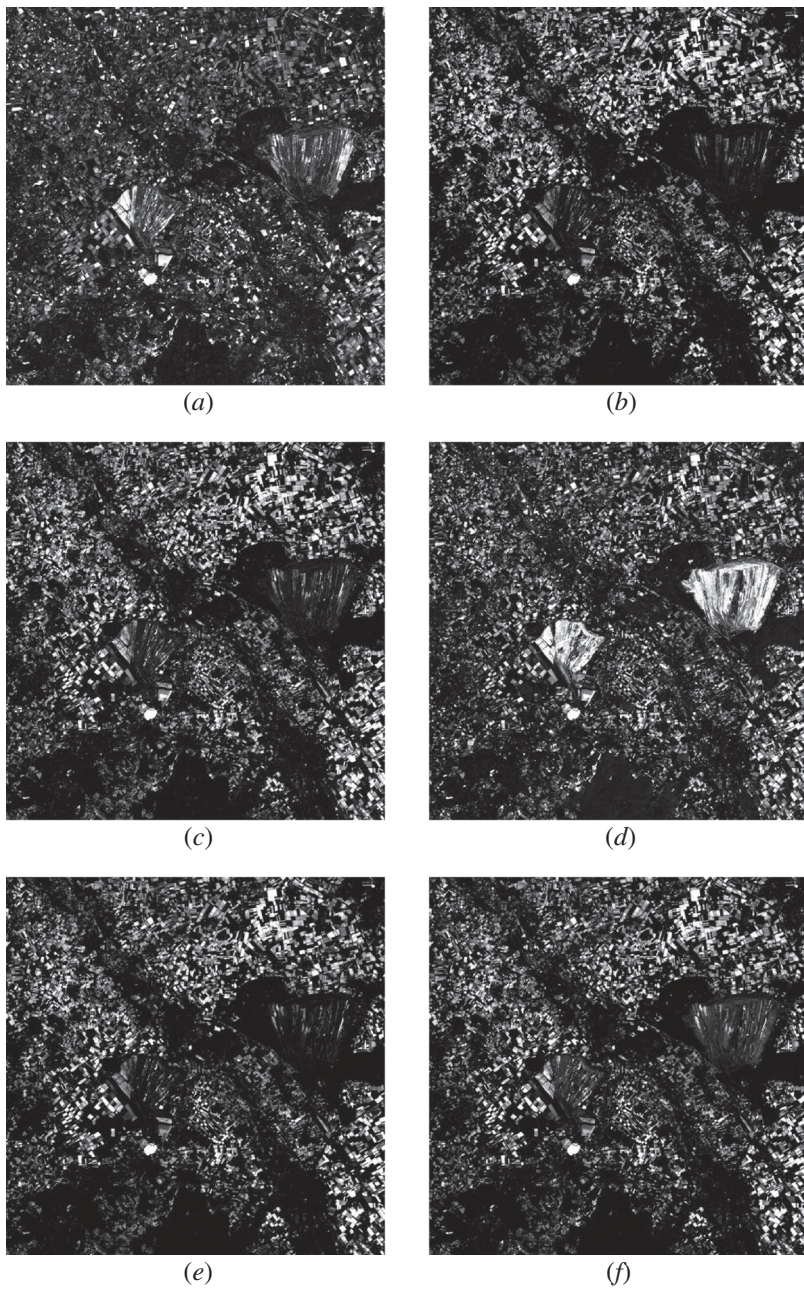


**Figure 7.** Chi-square images computed for the German data set using (a)–(c) IR-MAD and (d)–(f) ITPCA, considering the cases where: (a), (d) ICM is not used (note the incorrect estimation of the unchanged regions); (b), (e) ICM based on the threshold of bin differences is used; (c), (f) ICM based on the first principal component is used. The change is proportional to the grey value, where black denotes no change.

better identified with respect to the case where ICM is not used. This means that masking even a small portion of the strongest changes helps in improving radiometric normalization of the multi-temporal data set.



**Table 1.** Change detection results obtained by applying IR-MAD and ITPCA with and without the ICM on the German data set. The results are given for both ICM strategies ('hist' denotes the method based on the threshold of bin differences, and 'PCA' that based on the analysis of the first principal component). The table shows the detected changes, 'DC', the false alarms, 'FA', the missed alarms, 'MA', and the overall error, 'OE', in number of pixels.

Approach	DC (pixels)	FA (pixels)	MA (pixels)	OE (pixels)
IR-MAD without ICM	7928	2480	1593	4073
IR-MAD with ICM (hist)	9102	420	419	839
IR-MAD with ICM (PCA)	9007	428	514	942
ITPCA without ICM	8289	4125	1232	5357
ITPCA with ICM (hist)	9083	556	438	994
ITPCA with ICM (PCA)	8915	971	606	1577

The software offers the potential to plot the transformation line computed by ITPCA. Figure 8 shows the case in which ICM is not used, leading to an incorrect transformation, while Figure 9 shows the case in which ICM is used and a better correlation line is obtained.

In order to perform quantitative analysis, a reference map (Figure 4(c)) used in Marpu, Gamba, and Canty (2011) is considered to validate the change detection maps obtained by thresholding the chi-square images. The thresholds between the change and no-change classes are identified by exploiting the EM algorithm, which is used to estimate class distribution in the chi-square images. Figure 10 shows the change detection map obtained by thresholding the chi-square images shown in Figure 7 obtained by

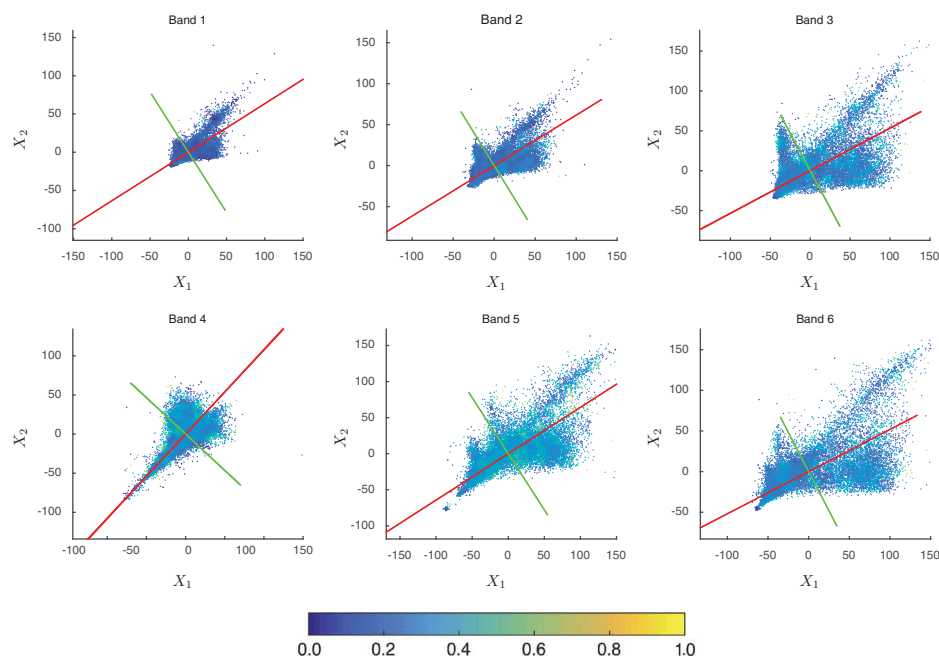


**Figure 8.** Density scatter plots of the six considered bands of the German data set after radiometric normalization performed using ITPCA, without ICM. Note the incorrect identification of the correlation line, which corresponds to the direction of the first principal component. The computation is affected by the inclusion of the changed pixels. The plots are computed considering 20,000 samples randomly selected, with the colour scale representing the data density.

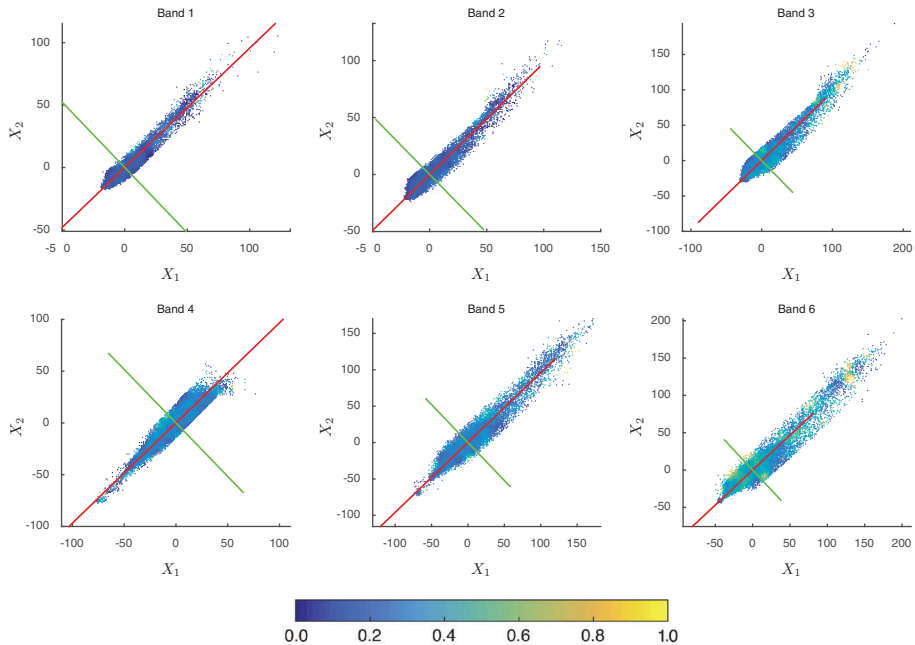


**Figure 9.** Density scatter plots of the six considered bands of the German data set after radiometric normalization performed using ITPCA and ICM. Note that ICM helps in finding a more correct linear relation. The plots are computed considering 20,000 samples randomly selected, with the colour scale representing data density.

performing IR-MAD and ITPCA. The results show the improvement when ICM is used, providing better results in terms of the number of changed pixels correctly detected and, at the same time, decreasing both the false and missed alarms (Table 1).

Although the presented methodology is unsupervised and does not require reference data, the software offers the potential to compute the receiver operating characteristic (ROC) in case reference data are available. For a given threshold computed on the chi-square image, the ROC curve shows the performance by comparing two operating characteristics, the true positive rate and the false positive rate. Optimal results are represented by the threshold that maximizes the true positive rate while minimizing the false positive rate. Such threshold is identified as the point on the curve that is closest to the upper-left corner. For demonstration, ROC curves computed on the obtained chi-square images considering the reference map (Figure 4(c)) are shown in Figure 11. One can see that the behaviour of the curves reflects the quantitative results obtained by applying the unsupervised threshold based on the EM algorithm, showing major improvement in change detection results when pre-processing is performed.

#### 4.4. Post-processing analysis

In order to show the results of post-processing related to minimization of misregistration errors based on the WRM approach, the Indonesian data set is considered. Figure 12 shows the chi-square images obtained using IR-MAD with ICM. It is

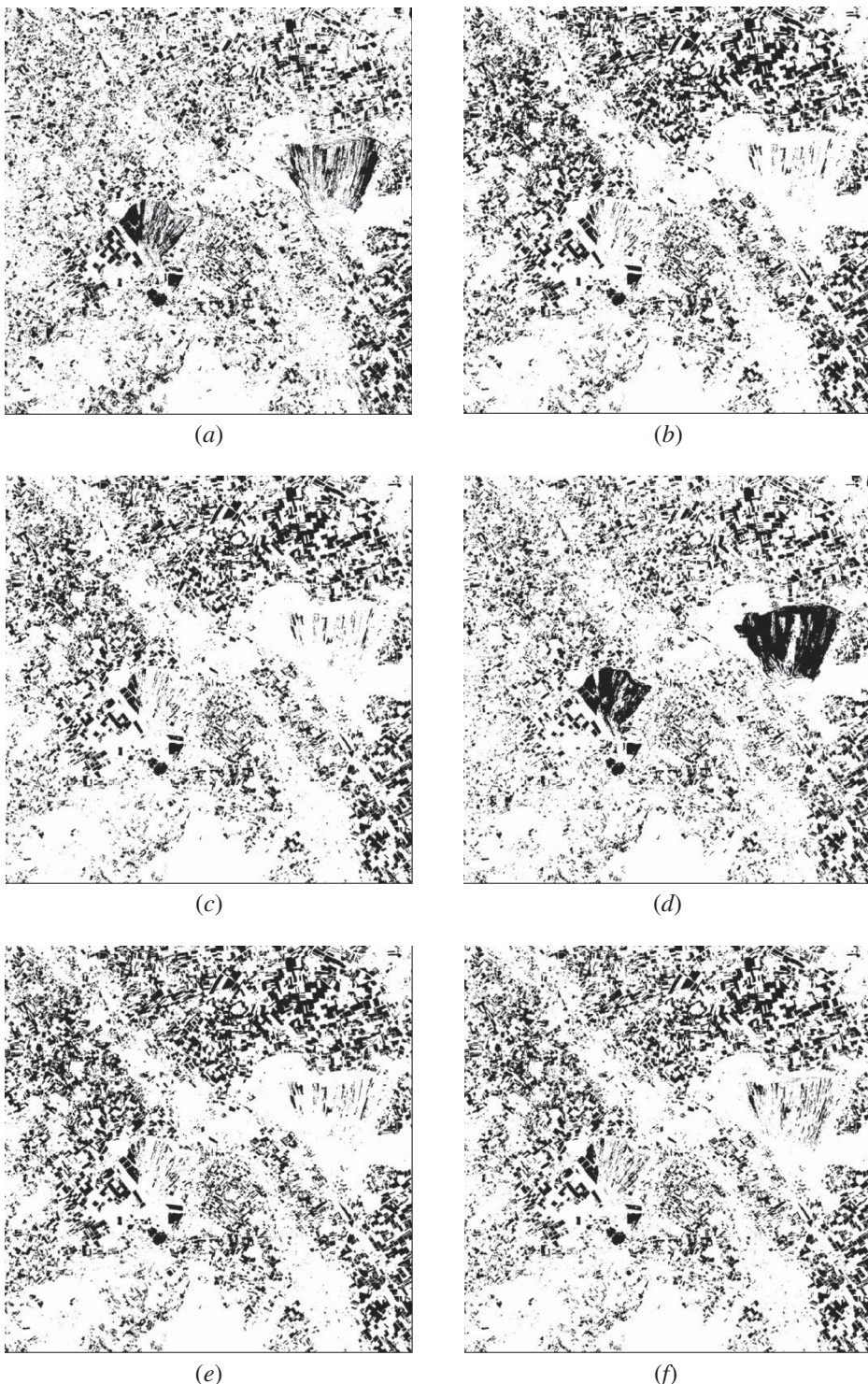


**Figure 10.** Change detection maps computed for the German data set using (a)–(c) IR-MAD and (d)–(f) ITPCA by thresholding the chi-square images shown in Figure 7. The change class is shown in white.

COLOUR  
FIGURE

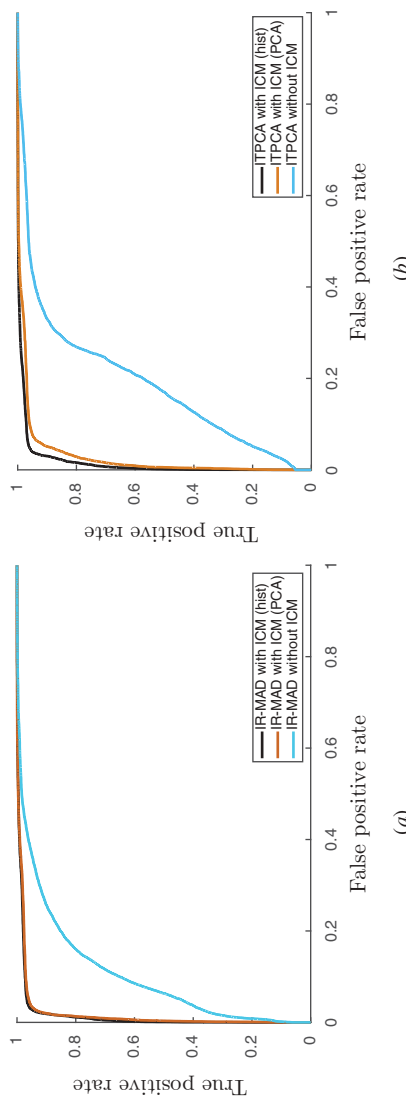
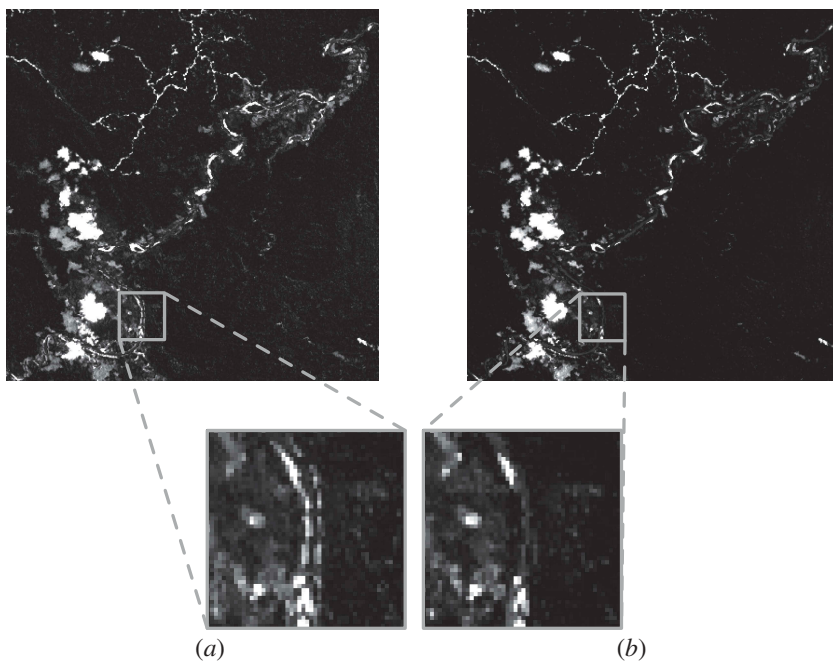


Figure 11. ROC curves computed for the German data set considering the chi-square images obtained by applying (a) IR-MAD, (b) ITPCA.



**Figure 12.** Minimization of misregistration error performed for the Indonesian data set. Chi-square image obtained by performing IR-MAD with ICM and (a) without post-processing and (b) with WRM. Note the misregistration error in the region marked by the grey rectangle, which is related to the river edges.

possible to identify regions (e.g. the region shown in the grey rectangle) where the effect of misregistration is present. In the case of the considered region, which is related to the edges of the river that are not completely aligned after the co-registration process, it will be observed that this leads to the appearance of regions that are not correctly classified as change (Figure 12(a)). When applying the WRM step, it is important to choose an appropriate dimension of the floating window in order to minimize miregistration error, but at the same time to preserve the real changes. In the experiments, a window of size  $5 \times 5$  pixels has been chosen. This implies that the algorithm tries to identify optimal matching between the pixels within a distance of two pixels. In Figure 12(b) it will be noticed that the regions related to the river edges, which are identified as changes, disappear.

Table 2 shows the computation times of the main functions for both implementations. All the experiments were performed using a computer with Intel Core Duo 2.93-GHz CPU and 4 GB of RAM. As expected, when the Matlab workspace is not used (in-line), IR-MAD and ITPCA computation is slower than when it is used. However, this difference is quite small when compared to the processing time of the other main functions.

## 5. Conclusion

This paper presents a toolbox for unsupervised change detection analysis for multi- and hyperspectral images. The software, which was developed in the Matlab<sup>®</sup>

**Table 2.** Comparison of the CPU time required for the main functions between the conventional strategy and the in-line strategy. The table reports the average time and the standard deviation in seconds, computed on five trials performed on the German data set.

Function	CPU time (s)	
	Conventional	In-line
IR-MAD	5.1 ± 0.2	56.6 ± 1.6
ITPCA	2.9 ± 0.6	148.4 ± 11.8
ICM (hist)	40.7 ± 1.3	27.1 ± 0.2
ICM (PCA)	23.2 ± 0.2	32.0 ± 0.2
WRM	113.3 ± 0.7	113.8 ± 0.7
Chi-square-EM	132.3 ± 1.7	133.2 ± 0.6

environment, implements two well-known change detection techniques, IR-MAD and ITPCA, together with a number of improvements. These improvements include the implementation of two different strategies for the computation of the ICM, which is aimed at solving the issue of low number of unchanged pixels, the identification of the darkest regions, and the definition of a strategy based on a floating window to mitigate the effect of misregistration. An important feature of the presented toolbox is its capability to handle large data sets by implementing a line-by-line processing strategy, which is based on the use of the method of provisional means that allows us to compute the required statistics, such as the means and covariance matrices, without saving the entire data set in the workspace. This permits the analysis to run in the background and use of a minimum amount of available memory.

## Disclosure statement

No potential conflict of interest was reported by the authors.

## Funding

This work was supported by the Icelandic Research Fund (RANNIS) no. [110043021] of the University of Iceland.

## ORCID

Nicola Falco  <http://orcid.org/0000-0003-3307-6098>

## References

- Bazi, Y., L. Bruzzone, and F. Melgani. 2007. "Image Thresholding Based on the EM Algorithm and the Generalized Gaussian Distribution." *Pattern Recognition* 40 (2): 619–634. doi:[10.1016/j.patcog.2006.05.006](https://doi.org/10.1016/j.patcog.2006.05.006).
- Bovolo, F., and L. Bruzzone. 2007. "A Theoretical Framework for Unsupervised Change Detection Based on Change Vector Analysis in the Polar Domain." *Geoscience and Remote Sensing, IEEE Transactions on* 45 (1): 218–236. doi:[10.1109/TGRS.2006.885408](https://doi.org/10.1109/TGRS.2006.885408).

- Bruzzone, L., and D. F. Prieto. 2000. "Automatic Analysis of the Difference Image for Unsupervised Change Detection." *IEEE Transactions on Geoscience and Remote Sensing* 38 (3): 1171–1182. doi:10.1109/36.843009.
- Canty, M. J. 2006. *Image Analysis, Classification and Change Detection in Remote Sensing: With Algorithms for ENVI/IDL*. Boca Raton, FL: CRC Press.
- Canty, M. J. 2014. *Image Analysis, Classification and Change Detection in Remote Sensing: With Algorithms for ENVI/IDL and Python*. Boca Raton, FL: CRC Press.
- Canty, M. J., and A. A. Nielsen. 2006. "Visualization and Unsupervised Classification of Changes in Multispectral Satellite Imagery." *International Journal of Remote Sensing* 27 (18): 3961–3975. doi:10.1080/01431160500222608.
- Canty, M. J., and A. A. Nielsen. 2012. "Linear and Kernel Methods for Multivariate Change Detection." *Computers & Geosciences* 38 (1): 107–114. doi:10.1016/j.cageo.2011.05.012.
- Celik, T. 2009. "Unsupervised Change Detection in Satellite Images Using Principal Component Analysis and k-Means Clustering</formula>." *IEEE Geoscience and Remote Sensing Letters* 6 (4): 772–776. doi:10.1109/LGRS.2009.2025059.
- Celik, T., and M. Kai-Kuang. 2010. "Unsupervised Change Detection for Satellite Images Using Dual-Tree Complex Wavelet Transform." *IEEE Transactions on Geoscience and Remote Sensing* 48 (3): 1199–1210. doi:10.1109/TGRS.2009.2029095.
- Chen, C. H. 2007. *Signal And Image Processing for Remote Sensing*. Boca Raton, FL: CRC Press.
- Chen, J., X. Chen, X. Cui, and J. Chen. 2011. "Change Vector Analysis in Posterior Probability Space: A New Method for Land Cover Change Detection." *IEEE Geoscience and Remote Sensing Letters* 8 (2): 317–321. doi:10.1109/LGRS.2010.2068537.
- Dengsheng, L., L. Guiying, and E. Moran. 2014. "Current Situation and Needs of Change Detection Techniques." *International Journal of Image and Data Fusion* 5 (1): 13–38. doi:10.1080/19479832.2013.868372.
- Dixon, W. J. 1981. *BMDP Statistical Software*. Berkeley, CA: University of California Press.
- Falco, N., P. R. Marpu, and J. A. Benediktsson. 2012. "Comparison of ITPCA and IRMAD for Automatic Change Detection Using Initial Change Mask." In *Geoscience and Remote Sensing Symposium, 2012. IGARSS 2012. IEEE International*, 6769–6772. Munich: IEEE. July.
- Galassi, M., J. Davies, B. Gough, G. Jungman, P. Alken, and R. Ulerich. 2015. "GNU Scientific Library - Reference Manual 2.1." <https://www.gnu.org/software/gsl/manual/>
- Ghosh, A., N. S. Mishra, and S. Ghosh. 2011. "Fuzzy Clustering Algorithms for Unsupervised Change Detection in Remote Sensing Images." *Information Sciences* 181 (4): 699–715. doi:10.1016/j.ins.2010.10.016.
- Hotelling, H. 1936. "Relation Between Two Sets of Variates." *Biometrika* 28 (3/4): 321377. doi:10.1093/biomet/28.3-4.321.
- Lindquist, A., and G. Picci. 1996. "Canonical Correlation Analysis, Approximate Covariance Extension, and Identification of Stationary Time Series." *Automatica* 32 (5): 709–733. doi:10.1016/0005-1098(96)80649-2.
- Luo, W., and L. Hongliang. 2011. "Soft-Change Detection in Optical Satellite Images." *Geoscience and Remote Sensing Letters, IEEE* 8 (5): 879–883. doi:10.1109/LGRS.2011.2131632.
- Marchesi, S., and L. Bruzzone. 2009. "ICA and Kernel ICA for Change Detection in Multispectral Remote Sensing Images." In *Geoscience and Remote Sensing Symposium, 2009 IEEE International, IGARSS 2009*, Vol. II-980-II-983. Cape Town: IEEE.
- Marpu, P. R., P. Gamba, and J. A. Benediktsson. 2011. "Hyperspectral Change Detection Using IR-MAD and Feature Reduction." In *Geoscience and Remote Sensing Symposium, 2011. IGARSS 2011. IEEE International* 98-101. Vancouver, BC: IEEE.
- Marpu, P. R., P. Gamba, and M. J. Canty. 2011. "Improving Change Detection Results of IR-MAD by Eliminating Strong Changes." *Geoscience and Remote Sensing Letters, IEEE* 8 (4): 799–803. doi:10.1109/LGRS.2011.2109697.
- Nielsen, A. A. 2007. "The Regularized Iteratively Reweighted MAD Method for Change Detection in Multi- and Hyperspectral Data." *Image Processing, IEEE Transactions on* 16 (2): 463–478. doi:10.1109/TIP.2006.888195.

- Nielsen, A. A., K. Conradsen, and J. J. Simpson. 1998. "Multivariate Alteration Detection (MAD) and MAF Postprocessing in Multispectral, Bitemporal Image Data: New Approaches to Change Detection Studies." *Remote Sensing of Environment* 64 (1): 1–19. doi:[10.1016/S0034-4257\(97\)00162-4](https://doi.org/10.1016/S0034-4257(97)00162-4).
- Schaum, A., and A. Stocker. 1998. "Long-Interval Chronochrome Target Detection." In *Proc. 1997 International Symposium on Spectral Sensing Research*, 1760–1770.
- Schaum, A. P., and A. Stocker. 2004. "Hyperspectral Change Detection and Supervised Matched Filtering Based on Covariance Equalization." In *Proc. SPIE 5425, Algorithms and Technologies for Multispectral, Hyperspectral, and Ultraspectral Imagery X*, Vol. 542577–542590. Washington, DC: SPIE.
- Schowengerdt, R. A. 2007. *Remote Sensing: Models and Methods for Image Processing*. Academic Press.
- Theiler, J., and B. Wohlberg. 2012. "Local Coregistration Adjustment for Anomalous Change Detection." *IEEE Transactions on Geoscience and Remote Sensing* 50 (8): 3107–3116. doi:[10.1109/TGRS.2011.2179942](https://doi.org/10.1109/TGRS.2011.2179942).
- Townshend, J. R. G., C. O. Justice, C. Gurney, and J. McManus. 1992. "The Impact of Misregistration on Change Detection." *IEEE Transactions on Geoscience and Remote Sensing* 30 (5): 1054–1060. doi:[10.1109/36.175340](https://doi.org/10.1109/36.175340).
- Vokey, J. R., and S. W. Allen. 2011. *Thinking with Data*. Alberta: University of Lethbridge.
- Wiemker, R., A. Speck, D. Kulbach, H. Spitzer, and B. Johann. 1997. "Unsupervised Robust Change Detection on Multispectral Imagery Using Spectral and Spatial Features." *Proceedings of the Third International Airborne Remote Sensing Conference and Exhibition*, 7–10. July. Ann Arbor, MI : Environmental Research Institute of Michigan